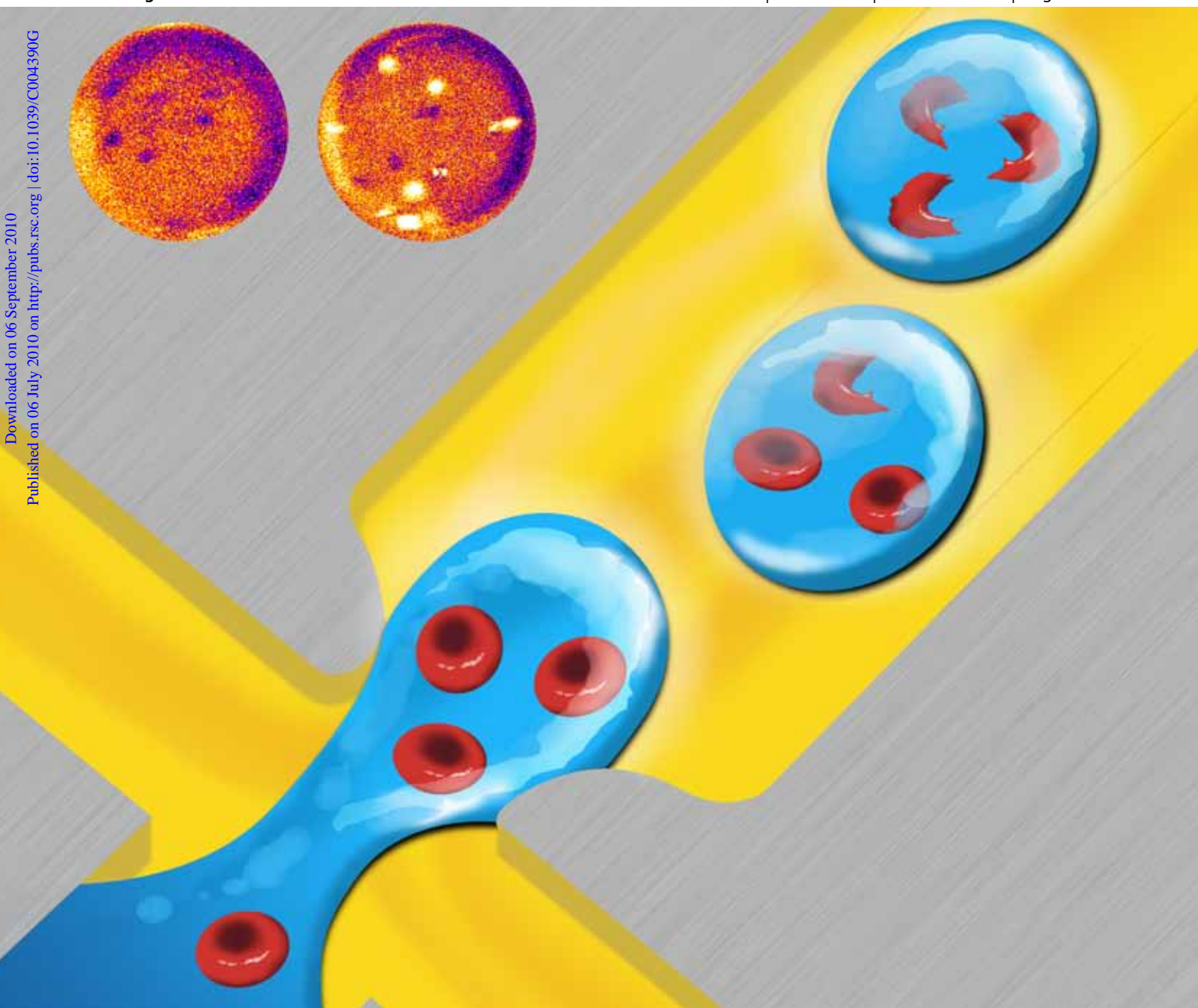


Lab on a Chip

Micro- & nano- fluidic research for chemistry, physics, biology, & bioengineering

www.rsc.org/loc

Volume 10 | Number 19 | 7 October 2010 | Pages 2481–2636



Downloaded on 06 September 2010
Published on 06 July 2010 on http://pubs.rsc.org | doi:10.1039/C004390G

ISSN 1473-0197

RSC Publishing

Baroud *et al.*
Sickling of red blood cells

Funatsu *et al.*
Thermoreversible gelation polymer

Whitesides *et al.*
Programmable diagnostic devices

Wooley *et al.*
Multibiomarker analysis

Sickling of red blood cells through rapid oxygen exchange in microfluidic drops†

Paul Abbyad,^{ab} Pierre-Louis Tharaux,^{cd} Jean-Louis Martin,^a Charles N. Baroud^{*b} and Antigoni Alexandrou^{*a}

Received 18th March 2010, Accepted 25th May 2010

DOI: 10.1039/c004390g

We have developed a microfluidic approach to study the sickling of red blood cells associated with sickle cell anemia by rapidly varying the oxygen partial pressure within flowing microdroplets. By using the perfluorinated carrier oil as a sink or source of oxygen, the oxygen level within the water droplets quickly equilibrates through exchange with the surrounding oil. This provides control over the oxygen partial pressure within an aqueous drop ranging from 1 kPa to ambient partial pressure, *i.e.* 21 kPa. The dynamics of the oxygen exchange is characterized through fluorescence lifetime measurements of a ruthenium compound dissolved in the aqueous phase. The gas exchange is shown to occur primarily during and directly after droplet formation, in 0.1 to 0.5 s depending on the droplet diameter and speed. The controlled deoxygenation is used to trigger the polymerization of hemoglobin within sickle red blood cells, encapsulated in drops. This process is observed using polarization microscopy, which yields a robust criterion to detect polymerization based on transmitted light intensity through crossed polarizers.

Introduction

Sickle cell anemia is a genetic disease that affects millions worldwide, particularly in sub-Saharan Africa and southern Asia. Patients who suffer from this disease experience painful crises, infections, or organ damage, leading to a shortened lifespan.¹ The condition is due to a single mutation on the beta chain of hemoglobin, the protein that is responsible for oxygen transport in the body. After oxygen is released in the tissues, a conformational change in mutant hemoglobin (HbS) exposes a hydrophobic residue on the surface of the protein that provokes hemoglobin polymerization. This in turn leads to red blood cells taking a “sickle” shape, from which the name derives, and greatly losing their deformability provoking vaso-occlusions.

Even though the literature on sickle cell anemia is extensive,^{2–7} microfluidics provides a novel approach for the study of key aspects of the disease which are not accessible by other techniques. The study of single cells, or a small number of cells, can be performed in microfluidic devices in an environment that mimics physiological conditions, in terms of mechanical shear of the cells,^{8,9} their interactions with the geometry,¹⁰ and chemical and biochemical signals. Among experimental conditions, oxygen partial pressure of the cell medium constitutes a key

parameter that must be controlled in order to trigger cell sickling. Existing techniques to provide such control use multi-layer microfluidic devices, where exchange occurs over the scale of seconds through a thin PDMS membrane separating flowing gas channels and aqueous channels.^{11,12} This exchange speed can be insufficient to study the dynamics of HbS polymerization in red blood cells, which occurs in less than a second after deoxygenation.¹³

The platform that we chose for performing the study uses water drops in oil. This approach allows many independent experiments to be performed in series, while providing a way for the cells' mechanical and biochemical environment to be precisely controlled. Indeed, it has been shown that cells can be encapsulated in aqueous drops that are only a few times their size,^{14–16} and whose composition and size are carefully controlled. Later, the drops can be sorted, fused, divided, or held in place through passive^{17–20} or active^{21–25} techniques. Furthermore, since a small number of cells can be enclosed in a droplet, this approach can serve as a general system to isolate and quantify the temporal behavior of single cells following changes in environment or addition of a chemical or biochemical reagent, especially in the case of non-adherent cells that need to remain suspended.

Most droplet applications have used the carrier oil as a passive transporter, with the primary function of forming and moving droplets within the device. However, the oil can also serve to extract or inject substrates,²⁶ while the surfactant it carries can catalyze a reaction at the drop–oil interface.²⁷ In our approach, the large surface to volume ratio of microfluidic drops provides a powerful lever to enhance the transfer between the two phases, aided by the convective flow that emerges from the presence of the immiscible interface. Here, we take advantage of the efficiency of the inter-phase transfer and present a novel method to provoke a rapid change in oxygen concentration within a microfluidic droplet, by using the oil phase as a source or sink

^aLaboratoire d'Optique et Biosciences (LOB), Ecole Polytechnique, INSERM U696, CNRS, 91128 Palaiseau, France. E-mail: antigoni.alexandrou@polytechnique.edu

^bLaboratoire d'Hydrodynamique (LadHyX) and Department of Mechanics, Ecole Polytechnique, CNRS, 91128 Palaiseau, France. E-mail: baroud@ladhyx.polytechnique.fr

^cParis-Cardiovascular Research Centre, INSERM U970, 56 rue Leblanc, 75015 Paris, France

^dCentre de Référence de la Drépanocytose, Hôpital Tenon, AP-HP, 4, rue de la Chine, 75970 Paris, France

† Electronic supplementary information (ESI) available: Supplementary Figure 1 and Movie 1. See DOI: 10.1039/c004390g

of oxygen. This is achieved through the use of perfluorinated oils which have been shown to be biocompatible^{16,28,29} and which have 10–20 times greater oxygen solubility than water.³⁰

The oxygen concentration of the oil and aqueous phases in our device are adjusted separately before entering the microchannel. To ensure that the oxygen transfer occurs solely within the microsystem, the device is made from a gas impermeable material, the photocurable glue NOA81,³¹ rather than a material such as PDMS that has high oxygen permeability and solubility.³² After the formation of droplets, the oxygen partial pressures of the two phases quickly equilibrate near the value for the oil, which has much greater capacity than water and is present in larger volumes, as in most droplet studies. By measuring the rates of oxygen transfer between the drops and the surrounding environment, we thus demonstrate that the carrier fluid can be used as a chemical reservoir in which the concentrations can be precisely varied. This should lead to the ability to perform sequential analysis of flowing droplets which contain red blood cells and should offer a method for quickly varying experimental conditions to explore therapeutics that inhibit cell sickling.

In this manuscript, we first describe the components required for oxygen control on the chip. This is followed by a characterization of the oxygen change for a droplet as a function of position and time using an oxygen sensing fluorescent probe. The time required to deoxygenate a droplet and the magnitude of the change are determined as a function of droplet size and speed. Finally, the device is used to provoke the polymerization of hemoglobin in red blood cells and show how the polymerized fibers can be detected, within the droplets, using polarized light microscopy.

Materials and methods

Microfluidic device fabrication

The microfluidic devices were made of photocurable glue following the protocol described by Bartolo *et al.*³¹ Briefly, a patterned PDMS stamp is made using standard soft lithography techniques.³³ The stamp is pressed over a drop of Norland Optical Adhesive 81 (NOA 81, Thorlabs) on a glass coverslide before exposure to a UV lamp (exposure for 40 s at an intensity of 7 mW cm⁻²). A thin layer of glue remains uncured on the surface due to the presence of oxygen, which allows the device to be sealed with a glass slide with a second exposure to a UV source (exposure for 40 s at an intensity of 7 mW cm⁻²). To render the internal channel surface hydrophobic, a glass treatment chemical (Aquapel, PPG Industries) is flowed briefly through the microchannel.

Two different chip geometries were used that had similar channel layout but different channel widths. The two geometries, henceforth referred to as narrow and wide, had channel widths of 120 and 250 μm , respectively, in the channels upstream of the droplet formation, and a channel width of 200 and 400 μm , respectively, downstream of drop formation (Fig. 1C). At a distance of 5 mm downstream of the flow focuser, the channel widens to 1 mm for the narrow channel and 2 mm for the wide channel. This widening was used to slow down the droplet flow speed to facilitate the observation of individual cells. The channel height was constant at 38 μm .

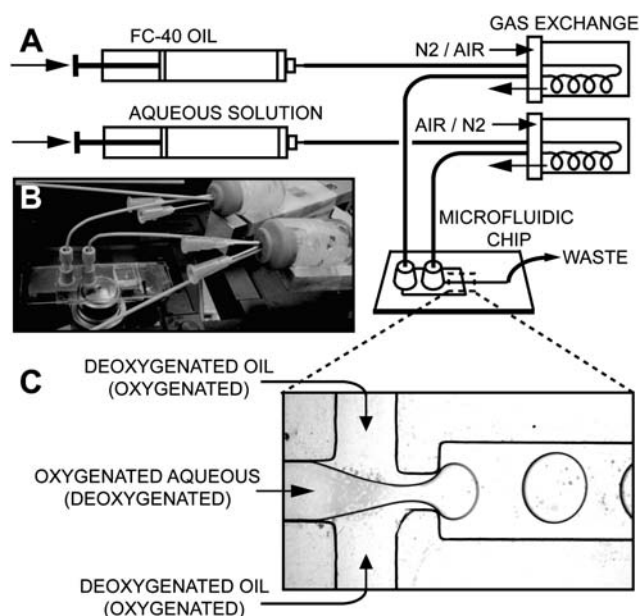


Fig. 1 (A) Schematic of the experimental setup. (B) Photograph of the gas exchange vials and the microfluidic device positioned above the microscope objective. (C) Close-up of the flow focuser and the aqueous droplet formation in the device (bright-field transmission image). By controlling the oxygen level of the incoming oil and aqueous phase, a change in the droplet oxygen concentration is obtained.

Experimental setup

A schematic of the experimental setup is shown in Fig. 1A. The aqueous phase and the oil (FC-40, graciously donated by 3M) are pushed at constant flow rates using glass syringes and syringe pumps. Flow rates ranged from 0.25 to 2 $\mu\text{L min}^{-1}$ for the aqueous phase and 2 to 16 $\mu\text{L min}^{-1}$ for the oil phase. To vary the oxygen concentration of the phases, the oil and aqueous solutions are first flowed through approximately 50 cm of gas permeable silicone tubing (0.5 mm internal diameter and 2.1 mm outer diameter, Cole-Parmer) in a vial with a controlled oxygen atmosphere. The residence time of the fluids in the exchange vials ranged from 6 min for the fastest flow rates (16 $\mu\text{L min}^{-1}$) to over 400 min for the slowest (0.25 $\mu\text{L min}^{-1}$). By varying the relative flow rates of nitrogen gas and air into each of the vials, the oxygen concentration in the vials could be adjusted from 0% to 21% oxygen (atmospheric oxygen percentage) *i.e.* from 0 to 21 kPa oxygen partial pressure ($p\text{O}_2$). Through gas exchange, the flowing fluids equilibrated with the oxygen partial pressure in the vials. After the gas exchange vials, it is important to maintain a virtually gas-tight environment. Therefore low gas permeability tubing made of polyether ether ketone (PEEK, Upchurch) was used to connect the vial to the NanoPort (Upchurch) inlets of the microfluidic device (Fig. 1B).

Figure 1C shows a photo of the flow-focusing junction where the oil and water meet and form droplets. Droplet size ranged from 130 to 190 μm for the narrow chip geometry and from 200 to 350 μm for the wide chip geometry. Two different initial conditions were characterized, “deoxygenation”, which corresponds to deoxygenated oil meeting an aqueous phase at ambient oxygen partial pressure, and “oxygenation” where ambient oxygen oil meets a deoxygenated aqueous phase. Here,

the terms oxygenation and deoxygenation refer to the change imposed to the aqueous droplet.

Determination of on-chip oxygen concentration

The on-chip oxygen concentration in the aqueous phase and in individual microdroplets was determined through the use of a probe, ruthenium tris(dipyridyl) dichloride hexahydrate (RTDP) (Sigma-Aldrich), whose fluorescence intensity and lifetime vary with the oxygen concentration.³⁴ The fluorescence lifetime was monitored using a commercial frequency-domain set-up (Ocean Optics FOXY) coupled directly to an inverted microscope (Zeiss AxioObserver). The system uses a bifurcated optical fiber to both output the excitation light and collect fluorescence. The excitation pulse at 470 nm, produced by a LED, was coupled into the microscope's epi-fluorescence path, where it was focused onto a small drop (for the calibration curve) or a microfluidic channel by a 100 \times objective (NA 1.4). The circular area of illumination had a diameter of approximately 200 μm . The resulting fluorescence, peaked at around 620 nm, was collected back into the fiber and analyzed by a multi-frequency phase fluorometer to determine the fluorescence lifetime.

The quenching of fluorescence by a collisional quencher such as oxygen is described by a first-order Stern–Volmer equation, $I_0/I = 1 + K_{SV}[\text{O}_2] = 1 + K'_{SV} p\text{O}_2$, where I_0 is the fluorescence intensity with no quencher (0% oxygen), K_{SV} is the Stern–Volmer constant and $[\text{O}_2]$ and $p\text{O}_2$ are the concentration and partial pressure of oxygen, respectively.³⁵ In the case of a mono-exponential fluorescence decay in time, as is the case for RTDP, the fluorescence lifetime can be substituted into the Stern–Volmer

equation: $\tau_0/\tau = 1 + K'_{SV} p\text{O}_2$, where τ_0 is now the fluorescence lifetime with no quencher.

A calibration curve to relate fluorescence intensity to oxygen partial pressure was obtained by exposing a 1–2 μL droplet of RTDP solution (1–2 mg mL^{-1} in deionized water) to an oxygen percentage from 0% to 21% (ambient oxygen percentage). A calibration curve was recorded before each experiment. The calibration curve was well described by the first-order Stern–Volmer equation (r^2 of the fit > 0.999). The RTDP fluorescence lifetime in aqueous solution ranged from 600 ns for 0% oxygen to 380 ns for 21% oxygen. The experimental K_{SV} was determined to be $2.1 \times 10^{-3} \mu\text{M}^{-1}$, similar to literature values of $2.7 \times 10^{-3} \mu\text{M}^{-1}$.^{36,37}

For the on-chip measurements, the aqueous phase consisted of RTDP solution (1–2 mg mL^{-1} in deionized water) and the oil phase was FC-40 with 2% w/w of surfactant. Measurements of fluorescence lifetime were made at discrete positions along the length of the microfluidic channel, both on the incoming aqueous stream and further downstream on aqueous droplets. The time-resolved fluorescence system has two modes of operation, intermittent and continuous. Most measurements were performed in intermittent mode where measurements were taken every 2 s with an integration time of 0.5 s. This integration represents the passage of several drops, from 2 to 25 drops depending on the specific flow conditions used in the experiment. In continuous mode, the excitation source is on at all times and the lifetime is determined every 0.1 s. This was found to be more accurate for the slowest droplet flow speeds although care must be taken to exclude data of low fluorescence when no droplets are present in the focal spot.

The measurements taken as a function of position were converted to measurements as a function of time. Upstream of the

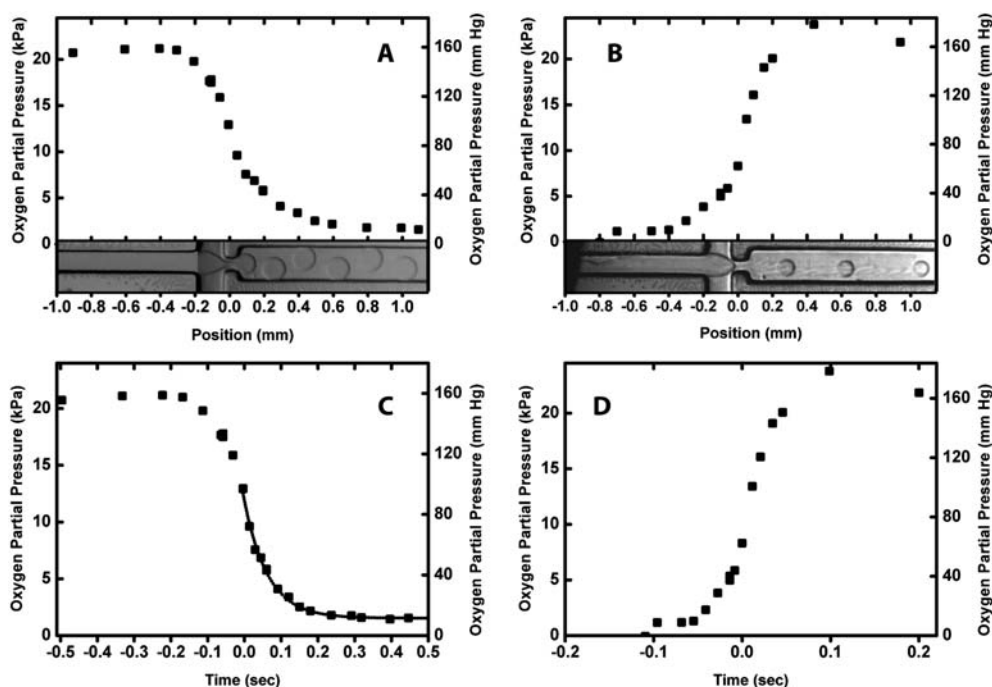


Fig. 2 Oxygen partial pressure ($p\text{O}_2$) as determined by RTDP fluorescence lifetime. (A) $p\text{O}_2$ with respect to position for an aqueous phase entering a stream of deoxygenated oil. The flow rate is $0.5 \mu\text{L min}^{-1}$ for the aqueous phase and $2 \mu\text{L min}^{-1}$ for the oil phase. (B) $p\text{O}_2$ with respect to position for a deoxygenated aqueous phase entering a stream of oil. The flow rate is $2 \mu\text{L min}^{-1}$ for the aqueous phase and $4 \mu\text{L min}^{-1}$ for the oil phase. (C, D) Same data as (A) and (B), respectively, with respect to time. Zero position and time are defined to be at the center of the flow focuser as indicated in the images at the bottom part of (A) and (B). An exponential fit to the data as shown in (C) is used to determine the deoxygenation time displayed in Fig. 3.

flow focuser, the corresponding time was calculated using the channel dimensions and the aqueous flow rate as imposed by the syringe pump. Given the parabolic flow profile in microfluidic channels, this corresponds to an average value. Downstream of the flow focuser where droplets flow in oil, video sequences were used to determine the time to position correspondence. The rate of deoxygenation was determined by fitting the oxygen concentration as a function of time to a single exponential decay with a variable offset. Only the section downstream of the flow focuser (position > 0 mm in Fig. 2A) and before the channel widening (position < 5 mm) was fitted.

Droplet diameter and speed were determined from image sequences. Droplets were fit to an ellipse and the diameter was taken as the average of the two ellipse axes. This procedure was chosen instead of a simple fit to a circle since larger droplets take on a slightly elongated shape in the oil flow. However, even in these cases, the two ellipse axes determined differed by less than 5%. The droplet speed was calculated by the displacement from successive image sequences. The droplet speed was sometimes slower immediately after the flow focuser, in which case the speed further downstream was used.

Sickling of red blood cells

Blood samples were obtained from untreated sickle cell patients (Tenon Hospital, Paris) and stored at 4 °C using sodium citrate as an anti-coagulant. Blood extracted from the authors was used in control experiments. Samples were used within a week after extraction. For static experiments on red blood cells, blood was diluted 200–500 fold in PBS buffer (137 mM NaCl, 2.7 mM KCl, 8.0 mM Na₂HPO₄, 1.5 mM KH₂PO₄, 5.5 mM glucose, 2 mM CaCl₂, pH 7.4). Three methods were used to deoxygenate at different rates the solution to provoke HbS polymerization. For slow deoxygenation, the atmosphere of a bell jar containing the diluted blood was exchanged over the course of several minutes with nitrogen gas. For deoxygenation in a few seconds, the oxygen was depleted enzymatically by adding glucose oxidase and catalase (Sigma-Aldrich) to diluted blood to final concentrations of 0.2 mg mL⁻¹ and 0.035 mg mL⁻¹, respectively.³⁸ To achieve deoxygenation in under a second, a small amount of sodium dithionite powder, which reacts efficiently with dissolved oxygen, was added directly to the diluted blood.

For on-chip experiments, the aqueous phase consisted of blood diluted 100–200 fold in D-PBS buffer (137 mM NaCl, 2.7 mM KCl, 8.0 mM Na₂HPO₄, 1.5 mM KH₂PO₄, 0.9 mM CaCl₂, 0.5 mM MgCl₂, pH 7.4, Invitrogen) and 35% v/v Optiprep (Sigma) to prevent cell sedimentation. Biocompatible surfactant, 0.5% dimorpholinophosphate-PFPE (DMP-PFPE)¹⁶ in FC-40, was added to the oil. The microfluidic chip was heated to 30 °C using a heater plate, thus approaching physiological temperatures.

Birefringence images were obtained with two crossed thin-film linear polarizers placed in the optical path of the microscope before and after the sample. The illumination source for the transmission measurements was a 100 W tungsten-halogen lamp (Zeiss) set to maximum luminosity with a blue-bandpass filter inserted directly after the light source, centered at 437 nm with a 40 nm full width at half maximum. Images were recorded with a CCD camera (Retiga-4000R, QImaging, 2048 × 2048 pixels, 20 MHz).

Results and discussion

Characterization of on-chip oxygen concentration

The oxygen concentration of the aqueous phase and water droplets was characterized by the oxygen-induced fluorescence quenching of RTDP. This approach is well-suited for measurements in a microchannel^{12,39} as it requires small volumes, does not consume oxygen and is biocompatible to the extent that it has even been used to image oxygen levels in live cells.⁴⁰ The use of a commercial frequency-domain set-up for the lifetime measurements offers an inexpensive and accurate way to measure oxygen within flowing microdroplets. Measurements of fluorescence lifetime, instead of intensity, are used since they are much more robust; they are unaffected by photobleaching, inhomogeneous illumination or changes in excitation intensity.³⁵

The oxygen concentration as a function of the position in the channel was charted by scanning the longitudinal direction of the channel, under droplet deoxygenating conditions (Fig. 2A) and droplet oxygenating conditions (Fig. 2B). In the former case, the degassed oil acts as an oxygen sink, in the latter as an oxygen donor. In both the deoxygenation and oxygenation cases, the curves have a sigmoidal shape and display a large magnitude of oxygen change. In deoxygenation conditions, the final droplet partial pressure is less than 1.5 kPa, a reduction of 20 kPa from its initial value. In oxygenation conditions, the final oxygen concentration of the droplet approaches the ambient value. The solubility of oxygen in the FC-40 and water under standard laboratory pressure (100 kPa) and temperature (25 °C) is 3.2 mM and 0.26 mM, respectively.⁴¹ Therefore, at equilibrium, oxygen will preferentially partition into the oil phase. This combines with the typical excess in volume of oil compared to water used in droplet experiments to ensure a dramatic change in oxygen concentration in the aqueous droplet.

It is helpful to divide the position axis of Fig. 2A and B into three zones that have very different interfaces for exchange: the incoming aqueous stream, the droplet formation area and, lastly, the droplet flow in the carrier oil. Little oxygen transfer takes place in the incoming stream, as much as 50% of the transfer in the droplet formation area, the remaining transfer occurring soon after droplet formation. The droplets equilibrate with the surrounding oil within a few droplet diameters of the flow focuser.

Understanding the dynamics of the transfers in detail is complex because each zone presents a distinct advection/diffusion ratio. This ratio is given by the Peclet number, which is defined as $Pe = UL/D$, where U is a characteristic velocity, L is a characteristic length scale, and D is the diffusion coefficient of oxygen (2×10^{-5} cm² s⁻¹ in both water and FC-40).⁴² The small amount of oxygen transfer upstream of the drop formation can be understood by calculating the characteristic length at which diffusion equilibrates with advection for oxygen, by setting $Pe = 1$. For our experimental velocities, this yields length scales of less than 1 μm, indicating that diffusion is inefficient in transporting oxygen molecules upstream. In contrast, a large amount of oxygen variation occurs during droplet formation. This large exchange can be explained by the flow focusing geometry which leads to high velocities and velocity gradients in the nozzle region, thus enhancing the molecular transport there.

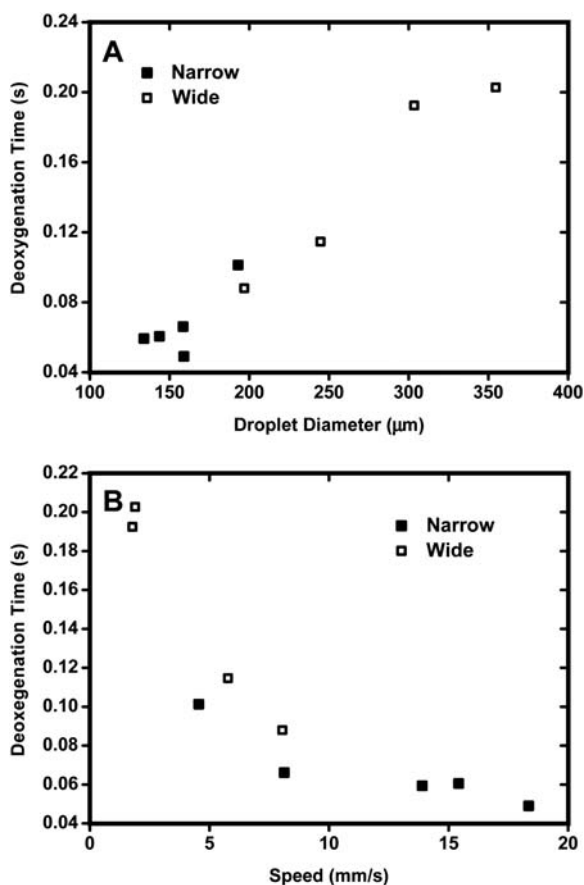


Fig. 3 Deoxygenation time as a function of (A) droplet diameter and (B) droplet speed. Two different geometries of chips were used and are labeled “narrow” and “wide”. Specifications on exact chip geometries are given in the Materials and methods section.

In addition to this enhanced transport, the neck connecting the droplet to the water inlet presents a long and slender shape that is favorable to rapid exchange through transverse diffusion. These different mechanisms add to the large diffusion coefficient of oxygen to produce rapid transfer of oxygen between the water and oil phases during the drop formation. Once the droplet forms, the high surface to volume ratio of the focused stream and droplet facilitates the exchange between the two phases, in addition to the further enhancement by the external and internal mixing flows.

In Fig. 2C and D the data with respect to position has been converted to time with the procedure detailed in the Materials and methods section. The data maintains an overall sigmoidal shape after the conversion to a time axis. In the examples of Fig. 2, the complete deoxygenation occurs in 0.4 s while the oxygenation takes 0.2 s because the droplets in the oxygenation example are smaller and faster than in the deoxygenation case. Under similar droplet conditions, oxygenation and deoxygenation show similar time dynamics (see supplementary Fig. 1C†).

The oxygen concentration as a function of time, after droplet formation (*i.e.* time > 0) was fit to a single exponential decay for different droplet sizes and speeds. The data were well fit by this function as shown by the example in Fig. 2C, thus yielding a characteristic time scale for the oxygen concentration variation.

The times thus obtained are shown in Fig. 3A and B, as a function of droplet diameter and speed, respectively. The values that we measure are in the range of 50 to 200 ms. The plot includes data obtained from two different chip geometries but the results are contiguous. The time for deoxygenation decreases for smaller and faster drops.

Molecular transport in microfluidic devices is often limited by diffusion, as previously reported in devices for oxygen control,^{10–12,39} where gas channels equilibrate with aqueous channels across thin PDMS membranes. Oxygen variations in these devices take place on the scale of seconds or more, determined by the diffusion of the oxygen molecules across the PDMS membrane and across

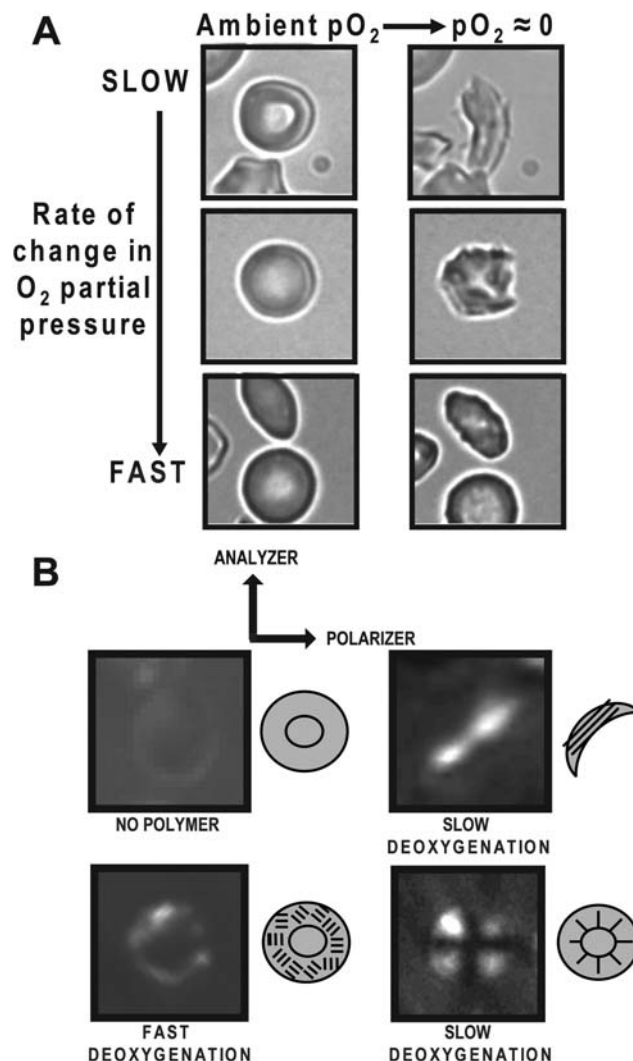


Fig. 4 (A) Correlation of sickle red blood cell shape with deoxygenation rate observed with static experiments. Top, slow deoxygenation (several minutes) by the exchange with nitrogen atmosphere. Middle, intermediate deoxygenation rate (several seconds) by the enzymatic oxygen consumption by glucose oxidase. Bottom, fast deoxygenation (sub-second) by addition of sodium dithionite directly to the sickle red blood cell solution. Images were taken with a 40 \times objective. (B) Sickle red blood cells observed with polarization microscopy. Directly to the right of the images is a schematic of the intracellular fiber orientation. The relative orientation of the crossed polarizers, is shown above the images. Images were taken with a 10 \times objective.

the height of the aqueous channel. In contrast, the oil in our devices, which acts as a gas reservoir, has a direct interface for exchange with the droplet. Therefore, the transport is expected to be much faster. Indeed, the relevant diffusion time in our system is given by $\tau_D = h^2/D$, where the height of the channels (h) gives the smallest droplet dimension. This would yield a value of 0.7 s for our microchannel geometry, independent of drop diameter or velocity.

The actual exchange times that we experimentally measure can be several times faster than this purely diffusive exchange time. The enhanced transfer can be understood by considering the presence of recirculation zones, inside and outside the drops, that are produced by the presence of the immiscible interface. This enhanced transport was recently studied in detail by Mary *et al.*²⁶ who found that droplet advection and shear enhanced diffusion significantly reduce exchange times with respect to simple diffusion, for values of the Peclet number similar to ours. In this context, the trends seen in Fig. 3 provide benchmarks to tune droplet size and speed to achieve a desired deoxygenation rate and point to ways of further optimizing the system.

Although multilayer devices may be more suitable for certain applications, such as the study of adherent cells, our system is well adapted to induce fast gas exchanges in drops and can be used in conjunction with the emerging technologies to sort, split, fuse and hold droplets.^{17–19,21–25} The results provided here show exchange times that are at least an order of magnitude faster than two-layer systems and can be further reduced if necessary. Below, we show how this control can be used to provoke HbS polymerization in droplet encapsulated red blood cells.

Sickling of red blood cells in a microfluidic device

This device was used to study the sickling of red blood cells by using the oil as an oxygen sink to perform the deoxygenation of the drops. In order to know what to expect in the droplet experiments, however, we first performed imaging of sickle cells under static conditions. The oxygen content of the cell medium was varied using gas exchange, enzymatic, or chemical deoxygenation, each corresponding to a different rate of deoxygenation. The typical change in cell morphology is shown in Fig. 4A, for the different experiments.

The rate of deoxygenation is a primary determinant of the cell shape upon sickling.¹³ For slow deoxygenation (over several minutes), the hemoglobin S forms unidirectional fibers that are of the length or longer than the size of the cell, leading to a drastic deformation of the cell (Fig. 4A, top). For a fast deoxygenation, in less than a second as occurs in our device, the hemoglobin in most cells will polymerize with a delay time of a few hundred milliseconds with almost no change in cell shape.¹³ It is only at high optical resolution (at least numerical aperture = 0.75) that an internal cobblestone appearance, indicative of small oriented polymer domains, is detected (Fig. 4A, bottom). These small polymer domains are very difficult to detect on-chip by bright field illumination due to the limited resolution and the tumbling motion of red blood cells within flowing drops.

Polarization microscopy offers a sensitive measure of polymer formation⁴³ that is compatible with imaging inside the microfluidic device. Sickled red blood cells are placed between crossed polarizers and illuminated with light whose wavelength is centered near the strong absorption of the Soret band of

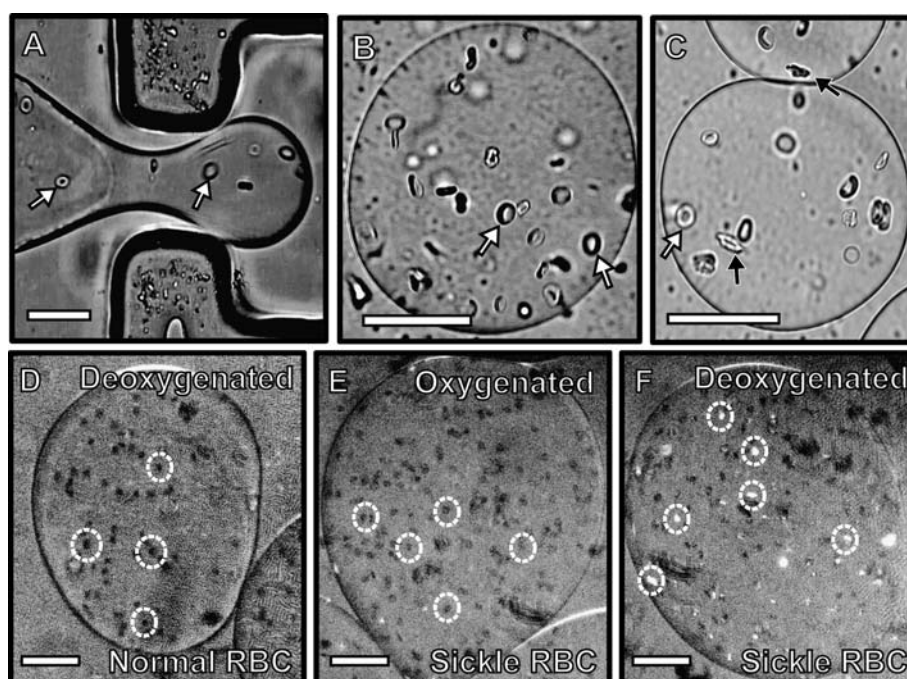


Fig. 5 (A–C) Bright-field transmission images taken at the flow focuser (A), for an oxygenated droplet (B), and a deoxygenated droplet (C). A few biconcave red blood cells are indicated with white arrows while black arrows indicate deformed red blood cells. Image (A) was taken with a 20× objective and (B) and (C) with a 40× objective. (D–F) Polarization microscopy images with a 10× objective of a deoxygenated droplet containing normal red blood cells (D), an oxygenated (E) and a deoxygenated (F) droplet containing sickle red blood cells. A few red blood cells in each image are circled in white. The scale bar represents 50 μm in all images.

hemoglobin (415 nm). The heme molecule, a planar molecule responsible for oxygen binding in hemoglobin, absorbs preferentially light polarized along its plane resulting in a linear dichroism and concomitant linear birefringence.⁴⁴ Therefore, aligned hemes, as found in hemoglobin S fibers, are birefringent and can induce a polarization rotation. In contrast, dissolved hemoglobin is found in random orientations and does not produce a polarization rotation. Therefore, a cell containing no fibers appears dark when placed between crossed polarizers (Fig. 4B, top left). However, once hemoglobin S fibers are formed within the cell, a polarization rotation is induced. This gives rise to a signal transmitted through the crossed polarizers which is most intense for fibers oriented at 45° to the polarizers. Furthermore, the signal is indicative of the intracellular fiber orientation such as radial, linear or in domains (Fig. 4B).

The observation of sickle cells on-chip is shown in Fig. 5. Figures 5A–C show bright field transmission images of sickle red blood cells at different positions within the channel. The image in Fig. 5A is taken at the flow focuser, as the aqueous stream is pinched off into droplets. The characteristic biconcave shape of individual red blood cells is clearly visible (see white arrows). Figures 5B and C show droplets observed at a fixed position downstream, corresponding to about 6 s after droplet formation. In Fig. 5B, both the droplet and oil were at ambient oxygen partial pressure and the red blood cells maintain their normal shape. In contrast, the droplet in Fig. 5C was deoxygenated by the carrier oil. The deoxygenation should provoke hemoglobin S polymerization in most cells and deformed cells can be discerned (see black arrows). However, several cells keep their normal shape while many are difficult to classify as sickle or normal from a static image. These images highlight some of the difficulties of determining sickling based solely on morphology in flowing droplets, in particular since a normal shape may appear sickled in certain orientations, for example if the cell is seen side-on. The analysis is also complicated by a small percentage of irreversibly sickle cells that remain deformed regardless of the oxygen partial pressure. However, the most serious obstacle is the aforementioned issue that most cells show only slight changes in cellular morphology upon rapid deoxygenation. Therefore, we expect that many of the cells shown in Fig. 5C contain hemoglobin S polymers but this cannot be discerned from the cell morphology.

These images are to be compared with the images obtained through polarization microscopy, shown in Fig. 5D–F. Again, these images are taken at a downstream position corresponding to 6 s after drop production, a long time compared with the time required to equilibrate oxygen with the surrounding oil. For a deoxygenated droplet containing normal red blood cells (Fig. 5D), the cells appear as dark spots over the dark gray background. The cells are also dark in the case of an oxygenated droplet containing sickle cells (Fig. 5E). In contrast, the sickle red blood cells in the deoxygenated drop appear as bright spots over the dark background (Fig. 5F), which yields a clear indication of the polymerization of the hemoglobin S molecule. These images demonstrate an easy way to distinguish cells containing polymerized vs. unpolymerized hemoglobin.

As a control experiment, the oil was cycled between an oxygenated and deoxygenated state, by changing the vial contents upstream of the microchannel, with all other

experimental conditions held constant (supplementary Movie 1†). By observing a steady stream of droplets at a fixed location, downstream of the flow focuser, the sickle red blood cells alternated between dark and bright with the oxygen partial pressure of the oil phase.

The objective classification criterion, dark *versus* bright cells, combined with the droplet deoxygenation strategy, provide a framework for a microfluidic device to study the red blood cell sickling under varying experimental and biochemical conditions.

Conclusions

We have demonstrated a single-layer system that can change the oxygen concentration of a flowing microdroplet using differential concentrations between the water and carrier oil phase. This device can provoke a drastic change in oxygen partial pressure in a microdroplet in less than 100 milliseconds, a time that can be further reduced by optimizing the channel geometry or by reducing the droplet size. We focused here on complete deoxygenation of the droplet, however intermediate oxygen concentrations can easily be achieved by controlling the initial oxygen level of the incoming oil.

The device was used to provoke the polymerization of hemoglobin S in red blood cells which was readily detected using polarization microscopy. This opens the way to studies on the parameters important for sickling of red blood cells, especially with regards to therapeutic agents that may inhibit hemoglobin S polymerization. Perfluorinated oils are known to dissolve a large collection of gases and therefore our device offers a general approach for gas exchange in droplets and can be used to inject a gaseous reactant to initiate a chemical reaction or biological process within a nanolitre droplet. Oil–droplet gas exchange thus provides a supplementary control of droplet content that can be combined with existing droplet technologies.

Acknowledgements

Special thanks to François Lionnet for providing blood from sickle cell patients and Jean-Christophe Baret for providing the perfluorinated surfactant used in our studies. We would also like to thank Marie-Claire Schanne-Klein for helpful discussions on the polarization measurements. We also gratefully acknowledge useful discussions with Cédric Bouzigues and Jeremy J. Agresti. This project was partially supported by Region Ile-de-France Nanosciences Competence Center. P.A. acknowledges financial support from CNRS and Ecole Polytechnique.

References

- 1 M. Stuart and R. Nagel, *Lancet*, 2004, **364**, 1343–1360.
- 2 L. Pauling, H. Itano, S. Singer and I. Wells, *Science*, 1949, **110**, 543–548.
- 3 A. Mozzarelli, J. Hofrichter and W. Eaton, *Science*, 1987, **237**, 500–506.
- 4 O. Platt, B. Thorington, D. Brambilla, P. Milner, W. Rosse, E. Vichinsky and T. Kinney, *New Engl. J. Med.*, 1991, **325**, 11.
- 5 G. Serjeant, *Lancet*, 1997, **350**, 725–730.
- 6 S. Embury, *Microcirculation*, 2004, **11**, 101–113.
- 7 P. Vekilov, *Br. J. Haematol.*, 2007, **139**, 173–184.
- 8 M. Abkarian, C. Lartigue and A. Viallat, *Phys. Rev. Lett.*, 2002, **88**, 68103.
- 9 M. Abkarian and A. Viallat, *Soft Matter*, 2008, **4**, 653–657.

- 10 J. M. Higgins, D. T. Eddington, S. N. Bhatia and L. Mahadevan, *Proc. Natl. Acad. Sci. U. S. A.*, 2007, **104**, 20496–20500.
- 11 A. P. Vollmer, R. F. Probst, R. Gilbert and T. Thorsen, *Lab Chip*, 2005, **5**, 1059–1066.
- 12 M. Polinkovsky, E. Gutierrez, A. Levchenko and A. Groisman, *Lab Chip*, 2009, **9**, 1073–1084.
- 13 W. Eaton and J. Hofrichter, *Blood*, 1987, **70**, 1245–1266.
- 14 A. Huebner, M. Srisa-Art, D. Holt, C. Abell, F. Hollfelder, A. DeMello and J. Edel, *Chem. Commun.*, 2007, 1218–1220.
- 15 S. Köster, F. E. Angilè, H. Duan, J. J. Agresti, A. Wintner, C. Schmitz, A. C. Rowat, C. A. Merten, D. Pisignano, A. D. Griffiths and D. A. Weitz, *Lab Chip*, 2008, **8**, 1110–1115.
- 16 J. Clausell-Tormos, D. Lieber, J. C. Baret, A. El-Harrak, O. J. Miller, L. Frenz, J. Blouwolf, K. J. Humphry, S. Köster, H. Duan, C. Holze, D. A. Weitz, A. D. Griffiths and C. A. Merten, *Chem. Biol.*, 2008, **15**, 427–437.
- 17 G. Cristobal, J. P. Benoit, M. Joanicot and A. Ajdari, *Appl. Phys. Lett.*, 2006, **89**, 034104.
- 18 M. Chabert and J. L. Viovy, *Proc. Natl. Acad. Sci. U. S. A.*, 2008, **105**, 3191.
- 19 A. Huebner, D. Bratton, G. Whyte, M. Yang, A. Demello, C. Abell and F. Hollfelder, *Lab Chip*, 2009, **9**, 692.
- 20 C. Schmitz, A. Rowat, S. Köster and D. Weitz, *Lab Chip*, 2009, **9**, 44–49.
- 21 M. Chabert, K. D. Dorfman and J. L. Viovy, *Electrophoresis*, 2005, **26**, 3706–3715.
- 22 K. Ahn, J. Agresti, H. Chong, M. Marquez and D. A. Weitz, *Appl. Phys. Lett.*, 2006, **88**, 264105.
- 23 C. N. Baroud, J. P. Delville, F. Gallaire and R. Wunenburger, *Phys. Rev. E*, 2007, **75**, 046302.
- 24 C. N. Baroud, M. R. de Saint Vincent and J.-P. Delville, *Lab Chip*, 2007, **7**, 1029–1033.
- 25 M. L. Cordero, D. R. Burnham, C. N. Baroud and D. McGloin, *Appl. Phys. Lett.*, 2008, **93**, 034107.
- 26 P. Mary, V. Studer and P. Tabeling, *Anal. Chem.*, 2008, **80**, 2680–2687.
- 27 A. Theberge, G. Whyte, M. Frenzel, L. Fidalgo, R. Wootton and W. Huck, *Chem. Commun.*, 2009, 6225–6227.
- 28 C. Holtze, A. C. Rowat, J. J. Agresti, J. B. Hutchison, F. E. Angile, C. H. J. Schmitz, S. Koster, H. Duan, K. J. Humphry, R. A. Scanga, J. S. Johnson, D. Pisignano and D. A. Weitz, *Lab Chip*, 2008, **8**, 1632–1639.
- 29 E. Brouzes, M. Medkova, N. Savenelli, D. Marran, M. Twardowski, J. Hutchison, J. Rothberg, D. Link, N. Perrimon and M. Samuels, *Proc. Natl. Acad. Sci. U. S. A.*, 2009, **106**, 14195.
- 30 J. Riess and M. Le Blanc, *Pure Appl. Chem.*, 1982, **54**, 2383–2406.
- 31 D. Bartolo, G. Degré, P. Nghe and V. Studer, *Lab Chip*, 2008, **8**, 274–279.
- 32 T. Merkel, V. Bondar, K. Nagai, B. Freeman and I. Pinnau, *J. Polym. Sci., Part B: Polym. Phys.*, 2000, **38**, 415–434.
- 33 D. C. Duffy, J. C. McDonald, O. J. A. Schueller and G. M. Whitesides, *Anal. Chem.*, 1998, **70**, 4974–4984.
- 34 O. Wolfbeis, L. Weis, M. Leiner and W. Ziegler, *Anal. Chem.*, 1988, **60**, 2028–2030.
- 35 J. Lakowicz, *Principles of Fluorescence Spectroscopy*, Kluwer Academic/Plenum Publisher, New York, 1999.
- 36 H. Gerritsen, R. Sanders, A. Draaijer, C. Ince and Y. Levine, *J. Fluoresc.*, 1997, **7**, 11–15.
- 37 D. Sud, G. Mehta, K. Mehta, J. Linderman, S. Takayama and M. Mycek, *J. Biomed. Opt.*, 2006, **11**, 050504.
- 38 H. Kueh, W. Brieher and T. Mitchison, *Proc. Natl. Acad. Sci. U. S. A.*, 2008, **105**, 16531.
- 39 G. Mehta, K. Mehta, D. Sud, J. Song, T. Bersano-Begey, N. Futai, Y. Heo, M. Mycek, J. Linderman and S. Takayama, *Biomed. Microdevices*, 2007, **9**, 123–134.
- 40 W. Zhong, P. Urayama and M. Mycek, *J. Phys. D: Appl. Phys.*, 2003, **36**, 1689–1695.
- 41 G. Takeshi, M. Gaku and K. Ken-Ichi, *Biochem. Eng. J.*, 2001, **8**, 165–169.
- 42 R. O'Brien, A. Langlais and W. Seufert, *Science*, 1982, **217**, 153.
- 43 W. Eaton and J. Hofrichter, *Adv. Protein Chem.*, 1990, **40**, 63.
- 44 J. Hofrichter, D. Hendrickson and W. Eaton, *Proc. Natl. Acad. Sci. U. S. A.*, 1973, **70**, 3604–3608.